Fuel 97 (2012) 174–185

Contents lists available at SciVerse ScienceDirect

Fuel

journal homepage: www.elsevier.com/locate/fuel

The influence of salinity on the viscous instability in viscous-modified low-interfacial tension flow during surfactant–polymer flooding in heavy oil reservoirs

Benyamin Yadali Jamaloei [a,b,*], Riyaz Kharrat [b], Koorosh Asghari [a,1]

[a] Petroleum Systems Engineering Department, Faculty of Engineering and Applied Science, The University of Regina, Regina, Saskatchewan, Canada
[b] Petroleum Research Center, Petroleum University of Technology, Tehran, Iran

ARTICLE INFO

Article history:
Received 5 February 2011
Received in revised form 20 February 2012
Accepted 21 February 2012
Available online 7 March 2012

Keywords:
Viscous instability
Oil-wet
Surfactant–polymer flooding
Heavy oil recovery
Capillary number

ABSTRACT

In this study, the effect of viscous instability at varying salinities of the displacing non-wetting phase (i.e., surfactant–polymer solution) in surfactant–polymer flooding of heavy oil reservoirs– which is a viscous-modified low-interfacial tension (IFT) flow through an initially preferential oil-wet porous medium– is quantified in the presence of the adverse mobility ratio. The dynamic mean pore-scale capillary number values are determined using two different approaches. The first approach is a Pore network approach (PNA) that excludes the viscous instability effects. The second approach is using the Viscous instability model (VIM) proposed by Peters and Flock [49] in which the concept of the wavelength of the viscous fingers is introduced. Afterwards, these two dynamic mean pore-scale capillary number values are compared to each other to highlight the effects of viscous instability at different salinity levels of the surfactant–polymer solution. The results show that including the viscous instability effects in the qualitative and quantitative evaluations of the viscous-modified low-IFT flow is vital. In particular, the viscous instability effects become more complex near the breakthrough of the displacing non-wetting phase. Furthermore, the effects of the salinity on the dynamic mean pore-scale capillary number (by excluding/excluding the viscous instability effects, i.e., from PNA and VIM, respectively), IFT, dynamic viscosity, contact angle, displacement front configuration, wavelength of the viscous fingers, dynamic values of the desaturated displaced wetting phase, breakthrough time, and the time of infinite injected pore volume is discussed in the surfactant–polymer flooding of an initially preferential oil-wet porous medium containing heavy oil.

1. Introduction and literature survey

Fluid flow through porous media at low-interfacial tension (IFT) condition occurs in several applications including surfactant-based chemical enhanced oil recovery and clean-up of the contaminated soils using injection of the surfactant-based fluids. In the surfactant-based chemical enhanced oil recovery, the effects of several parameters on its performance have been examined in the past. For a thorough literature survey, the reader is referred to the reviews provided elsewhere [1–6]. Here we solely provide a literature survey regarding the effect of salinity in the surfactant-based chemical enhanced oil recovery.

1.1. Literature survey

One of the most severe limitations of the surfactant-based chemical flooding is its performance sensitivity to the salinities of the injected chemical solution and the reservoir fluids. Several studies have been conducted in the past to address these issues. The most important studies in the 1970s regarding the effect of salinity on the surfactant-based chemical flooding are those of Bansal and Shah [7,8], Glover et al. [9], and Gupta et al. [10]. The effects of divalent ions have been investigated by Bansal and Shah [7]. They reported an increase in the IFT with increasing $CaCl_2$ (or $MgCl_2$) concentration in connate water. Bansal and Shah [8] reported a decrease in the optimum salinity (in terms of NaCl concentration) by the increase in the divalent ions concentration. Glover et al. [9] pointed out that the optimal salinity is not constant in brines containing divalent ions. They also concluded that the phase trapping can result in large retention of surfactant in a system that is at optimal salinity at the injected conditions. Glover et al. [9] and Gupta et al. [10] reported that the overoptimum

* Corresponding author. Address: Department of Chemical and Petroleum Engineering, The University of Calgary, 2500 University Drive NW, Calgary, AB, Canada T2N 1N4.
E-mail address: byadalij@ucalgary.ca (B. Yadali Jamaloei).
[1] Present address: Husky Energy Inc., Calgary, AB, Canada.

0016-2361/$ - see front matter © 2012 Elsevier Ltd. All rights reserved.
doi:10.1016/j.fuel.2012.02.050

salinity is not desirable in the drive water as it results in the surfactant partitioning into the trapped oleic phase.

The research on the effect of salinity in the surfactant-based chemical enhanced oil recovery continued in the 1980s. An understanding of the displacement mechanisms for a three-component, two-phase system as a function of phase behavior and injection composition was provided by Hirasaki [11]. His work aided in the interpretation of salinity gradient phenomenon. Celik et al. [12] showed that the precipitation, followed by redissolution at higher surfactant concentrations occurs as a result of the interaction between the divalent ions and petroleum sulfonates. Hirasaki [13] proposed a method by which the optimal salinity can be expressed through an appropriate intensive variable rather than overall surfactant concentration. In this method, the association of the alcohol is described by partition coefficients for distribution of the alcohol among brine, oil, and surfactant, and the association of sodium and divalent ions with surfactant is described by the Donnan equilibrium model. Kraft and Pusch [14] found that in high salinity reservoir systems the length and profile of the oil bank is controlled by phase conditions and viscous forces in the transition zone of the mobility buffer. They also concluded that by addition of a suitable alcohol as a cosolvent the temperature range of the stable displacement process could be extended without loss of recovery efficiency. Nelson [15] provided direct evidence that oil, not rock, plays the major role in trapping surfactant under high-salinity conditions. Hirasaki et al. [16] used a one-dimensional six-component finite-difference simulator to compare a salinity gradient design with a constant salinity design. They used the numerical dispersion to evaluate the effects of dispersive mixing and showed that, with a salinity gradient, change of phase behavior with salinity can be used to keep surfactant in the active region and to minimize retention. A surfactant system was formulated by Sharma and Shah [17] for a water-flooded reservoir at 80 °C with salinity in the range of 20–30 g/L. They found that the choice of alcohol and its partitioning behavior are important criteria for designing formulations for these reservoir conditions. Kumar et al. [18] showed that the IFT of dilute petroleum sulfonate solutions against oil increases dramatically upon additions of calcium or magnesium salts. Kumar et al. [19] documented the effects of divalent ions within the connate water on the coalescence behavior of oil droplets in surfactant formulations. They found that addition of divalent cations to sodium-based petroleum sulfonate–lignosulfonate solutions strongly influences the coalescence behavior of the oil droplets. The association of surfactant micelles with sodium and calcium ions was addressed by Hirasaki and Lawson [20]. Pithapurwala et al. [21] formulated a surfactant system for temperatures of up to 80 °C and salinity of 2–3% NaCl. They blended a petroleum sulfonate with a phosphated ester, which increased the salt tolerance of the petroleum sulfonate system. Leung and Shah [22] studied the solubilization and phase equilibria of water-in-oil microemulsions to explain how the molecular structure of various components of microemulsions and salinity influence the spontaneous curvature and elasticity of interfacial films. Finally, a theoretical model was developed by Chou and Bae [23], which includes the effects of salinity. The developed model can quantitatively predict the phase behavior of the surfactant formulations mixed with oil.

Some works have also been conducted in the 1990s, which have focused on the effects of divalent ions [24], salinity contribution to optimum formulation of microemulsions [25], IFT between saline water and hydrocarbon systems [26], concept of effective salinity [27], surfactant combinations at high salinities [28], effect of salinity on the critical micelle concentration of surfactants [29], alternatives to the salinity gradient for controlling dispersion [30], role of drive-water salinity in minimizing phase trapping [31], effects of the salinity of the droplets on the solubility of water in microemulsions [32], competition between monovalent and divalent counterions [33], adsorption of surfactant mixtures in presence of seawater salinities [34], and the effect of salinity on associative thickener aqueous solution rheology [35]. Agharazi-Dormani et al. [24] explained that higher recoveries by surfactant injection, when the brine in the porous medium contained divalent ions, is due to complete or partial pore blockage by precipitates formed when the petroleum sulfonate encounters divalent ions. Anton and Salager [25] extended the correlation for optimum formulation in anionic surfactant–oil–water–alcohol systems to most sodium salts from monovalent to tetravalent and to their mixtures. A survey of the salinity of western Canadian carbonate reservoirs was conducted by Badakshan [26]. He established the effect of the ionic composition, when synthetic brines consisting of $NaHCO_3$ and Na_2SO4 are employed, on the IFT of pure hydrocarbon–water systems. Porzucek and Ramirez [27] calculated the optimal injection strategies for surfactant/polymer flooding using an improved version of a one-dimensional, compositional simulator. They concluded that previous studies consistently underestimated the optimal amount of surfactant to inject. Miller et al. [28] found that the problem of microemulsion formation of surfactant with the hydrocarbon may be solved by using dual surfactant systems. They proposed that the combinations of dual surfactant systems, consisting of alkane sulfonate and ether sulfonate, dissolved in brine to form a homogeneous dispersion at high salinities. Noll [29] found that the presence of electrolyte at a fixed temperature lowers the critical micelle concentration of the pure surfactant, dodceyltrimethylammonium bromide and, and increases the sharpness of the onset of micellization. A numerical simulation was used by Barker [30] in order to use a salinity gradient to counter the adverse effects of dispersion. He found that the inclusion of an alcohol in the chemical slug is a viable alternative to a salinity gradient. Maerker and Gale [31] reasoned that lowering the drive-water salinity helps to remobilize part of the adsorbed surfactant and to minimize microemulsion phase-trapping. Abuin et al. [32] investigated the solubility of water in water-in-oil microemulsions stabilized by cetyltrimethylammonium as a function of the salinity of the droplets, and the nature of the salt employed to modify it. They inferred that the results obtained from experiments, in which equivalent salinities were reached by addition of different salts, make it possible to differentiate salt effects from counterion-specific effects. Carlsson et al. [33] investigated the competition between mono- and divalent ions in the association of counterions to the headgroups of amphiphiles in one surfactant system with organic counterions and one with inorganic counterions. The adsorption of a dual surfactant system was examined by Fjelde et al. [34] at seawater salinity by static adsorption onto kaolinite, nonequilibrium long-term dynamic adsorption on a reservoir core, and dynamic slug injection in a Berea core. Finally, Kaczmarski et al. [35] studied the influence of surfactant and salinity on the associative thickener aqueous solution rheology.

Finally, after year 2000 the study of salinity effect has been an active area of research. Some of the most important works after year 2000 include those of Hou et al. [36], Ström et al. [37], Wang et al. [38], Al-Sahhaf et al. [39], Li et al. [40], Mitra and Ghosh [41], Para and Warszynski [42]. Hou et al. [36] discussed the effects of salinity and temperature on IFT for oil–water–mixed surfactant. They proposed that the surfactant-rich middle layer containing a dispersion of small special liquid crystals forms in order to get ultra-low IFT. The adsorption isotherms for a cationic divalent surfactant on negatively charged silica, both in the absence and in the presence of added salt, was reported by Ström et al. [37]. They showed that the results of their model, which is based on spherical aggregates, are in good agreement with the experimental results. Wang et al. [38] synthesized a surfactant material, with nonionic and anionic hydrophilic group and soluble in 30% NaCl brine, for high salinity formations where salting out or cloud point

phenomena are present. The synthesized surfactant showed good surface activity in brine with 1,00,000 mg/L salinity. Al-Sahhaf et al. [39] measured the IFTs for n-octane/water system, in a wide range of conditions existing in oil reservoirs, and correlated them to pressure, temperature, and salt concentration. A flooding agent for the alkaline/surfactant/polymer flooding was synthesized by Li et al. [40]. Their results show that the flooding agent is tolerant to salt up to 1,50,000 mg/L and to Ca^{2+} and Mg^{2+} to 5000 mg/L at 90 °C, with minimum IFT of 10^{-3} mN/m. The effects of salts containing monovalent and divalent ions on the binary coalescence of water drops in o-xylene and toluene, and ethylene glycol drops in toluene was studied by Mitra and Ghosh [41]. Finally, Para and Warszynski [42] investigated the effect of divalent sulfate anions and monovalent hydrosulfate anions, on the surface tension of cethyltrimethyl ammonium salts $C_{16}TABr$ (CTABr) and $C_{16}TAHSO_4$ ($CTAHSO_4$). They show that monovalent anions like Br^-, Cl^- or HSO_4^- ions decrease more effectively the surface tension of investigated surfactant than SO_4^{2-} ions.

1.2. Motivation and objective

From the provided literature survey, it can be concluded that most of the previous studies have focused on the chemistry of salinity effects on the performance of low-IFT flow, which occurs in surfactant-based chemical flooding. In this study, the emphasis is on the investigation of the effects of salinity of the surfactant–polymer solution on the physics of the viscous-modified low-IFT flow with adverse mobility ratio through an initially preferential oil-wet porous medium. These conditions are normally available in surfactant–polymer flooding of an initially preferential oil-wet reservoir that contains heavy oil. In particular, the effects of varying salinity of the injected surfactant–polymer solution (i.e., displacing non-wetting phase) on the viscous instability is examined. The main effort is to quantify the effect of viscous instability at varying salinities of the displacing non-wetting phase in the surfactant–polymer flooding of an initially preferential oil-wet porous medium containing heavy oil.

2. Experimental

The micromodel set-up is the same set-up that has been explained in previous studies [43–48]. West Paydar crude oil was used in this study. West Paydar is one of the oil fields located in western Iran. Properties of this crude oil are given in Table 1. In addition, SARA analysis shows that the weight percentage of saturated, aromatics, resins, and asphaltenes in the crude oil sample are 34.3, 38.9, 20.1, and 6.7, respectively. A petroleum sulfonate was used as the surfactant material. Its properties are given in Table 2. Composition of the injected displacing phase in each run is given in Table 3. Table 4 gives the physical properties of the injected displacing phase and the porous medium at different salinities. All measurements and experiments were conducted at constant temperature of 25 ± 0.2 °C. The detailed explanation of the measurements and the materials used in this work can be found elsewhere [3–5,44,45].

Table 1
Properties of the crude oil . (© 2010 Elsevier B.V, reproduced from Ref. [43] with permission)

Temperature (°C)	Density (kg/m^3)	Viscosity (mPa s)
15.5	933.2	142.0
21.1	929.9	101.8
25.0	927.4	80.6
26.7	926.2	74.9

First, pattern of the synthetic porous medium was designed, etched, and fused. A schematic of the synthetic porous medium is given in Ref. [43]. The details on designing, etching, and fusing procedures can be found elsewhere [48]. Physical properties of the synthetic porous medium are given in Table 5. The length and width of the micromodel are the dimensions of the glass plate on which the porous network pattern was etched. The pore diameter is the diameter of a single pore body in the porous network and the throat diameter is the diameter of a single pore neck that connects the pore bodies. The coordination number is the number of pore necks that are connected to a single pore body. It is a measure of the degree of porous network connectivity. Also, the aspect ratio is the ratio of pore-to-throat diameters. Absolute permeability is a measure of the ability of a single fluid to flow through the porous micromodel in the presence of single phase flow. Finally, the average etched thickness is a measure of the average depth of the porous network, which has been created during the etching process. The details on determination of these properties can be found in a previous publication [48]. A preferentially oil-wet porous medium was used in this study. It is worth noting that in this study it is assumed that the wettability of the porous medium is determined to a large extent by the first fluid contacting the porous medium, which is the heavy crude oil.

In order to conduct the experiments, first, the micromodel was saturated with the West Paydar crude oil. Then, the polymer-contained surfactant solution was injected into the micromodel at a constant injection flowrate of 0.0008 cm^3/min. High-resolution digital camera and microscope were used to continuously capture high-quality images of the displacement front. These images were then loaded into the SigmaScan® Pro for the image processing. A variety of information was extracted from the image processing in SigmaScan® Pro, including the oil recovery values, wavelength of the developed viscous fingers, and saturation distribution in the micromodel during the displacement. Further details in regard to the procedure of conducting experiments can be found in Ref. [47].

3. Theoretical foundation

In order to properly quantify the effects of the viscous instability at varying salinity of the displacing non-wetting phase on the physics of flow, two approaches are discussed in this section. In these two approaches, the dynamic mean pore-scale capillary number is predicted. The reason is that the dynamic mean pore-scale capillary number provides a means to predict the relative change of the viscous-to-the capillary forces. The first approach is a pore network approach where the potential effects of the viscous instability, which are the trapping and bypassing of the displaced phase (i.e., oil), are neglected. This approach is explained in Section 3.1. In the second approach, however, the potential effects of the viscous instability on the physics of flow are considered by utilizing the viscous instability model in two-phase immiscible displacement in porous media. This model has been explained in detail by Peters and Flock [49]. This approach is explained in Section 3.2.

3.1. Determination of the pore-scale capillary number using the pore network approach

The pore-scale capillary number (N_{c_1}) is defined as:

$$N_{c_1} = \frac{\mu_d v}{\sigma \cos\theta} \text{ , wherein } v = \frac{u}{\varphi} \quad (1)$$

where μ_d is the dynamic viscosity of the displacing non-wetting phase (Pa s), v is the average interstitial velocity of the displacing

Table 2
Properties of the petroleum sulfonate. (© 2010 Elsevier B.V., reproduced from Ref. [43] with permission)

Approximate equivalent weight	Active sulfonate content (wt.%)	Free oil (wt.%)	Water (wt.%)	Inorganic salts (wt.%)	Critical micelle concentration (wt.%)
380	54	16.1	17.8	3.3	0.90

Table 3
Composition of the injected displacing non-wetting phase in each run.

Run No.	Concentration of components in 1000 cm^3 of distilled water						
	Surfactant (cm^3)	Ethanol (cm^3)	Xanthan (mg)	Calcium chloride (g)	Strontium chloride (g)	Magnesium chloride (g)	Sodium chloride (g)
1	2.0	5.0	0.125	0	0	0	0
2	2.0	5.0	0.125	0.275	0.1	0.12	0.2925
3	2.0	5.0	0.125	2.75	1.0	1.2	2.925

Table 4
Physical properties of the displacing phase and the porous medium at different salinities.

Run No.	Viscosity (mPa s)	IFT with crude oil (mN m^{-1})	Contact angle (°)
1	5.2	0.082	124
2	4.3	0.090	126
3	2.3	0.109	129

non-wetting phase (m s^{-1}), σ is the displaced wetting phase–displacing non-wetting phase IFT (N m^{-1}), Θ is the contact angle (°), u is the Darcy (superficial) velocity, and ø is the porosity. It is noted that in this study, the contact angles were measured on a preferential oil-wet glass surface. In the above relationship, the average interstitial velocity of the displacing non-wetting phase, v is [50]:

$$v = \frac{Q_{inj}\sum_{i=1}^{n}\frac{1}{f(i)}}{A_t\, n} \quad \text{wherein, } A_t = hd_t \tag{2}$$

where Q_{inj} is the injection flowrate of the displacing non-wetting phase (m^3 s^{-1}), $f(i)$ is the number of pore throats in the direction of flow path, i is the flow path level indicator that corresponds to the positions that the displacement front has travelled in the pore network approach and it is used to track the trail of front, n is the number of the flow path levels passed by the displacement front at any time, A_t is the cross sectional area of one pore throat (m^2), h is the average etched thickness of the porous medium, and d_t is the pore throat size (m). To derive Eq. (2) for the average interstitial velocity of the displacing non-wetting phase, v the following assumptions have been made [50]:

1. During the flow of the displacing non-wetting phase, injection flowrate is equally divided between the pore throats in the flow path direction (see Fig. 1).
2. Major flow of the displacing non-wetting phase takes place in the mean flow path direction along the diagonal path connecting the injection and production ports where there is maximum pressure drop; this assumption is valid since visual observations of the flow of displacing non-wetting phase within porous medium supported this assumption (see Figs. 2–4).
3. The average interstitial velocity of the displacing non-wetting phase, v in Eq. (2) is the arithmetic average of the interstitial velocities within pore throats at each flow path level (i.e., for each "n", see Fig. 1).
4. The effect of phase trapping and bypassing, as the direct consequences of the viscous instability, on the configuration of the displacement front and the velocity distribution have been neglected.

In the above definition for the average interstitial velocity of the displacing non-wetting phase, $v, f(i)$ is dependent upon the assumed flow path mode for the surfactant solution.

In this pore network approach (see Fig. 1), it is assumed that the displacement front generally tends to preferentially propagate along and in both sides of the diagonal path connecting the injection and production ports. There is a maximum pressure drop along the diagonal path connecting the injection and production ports in a quarter five-spot model utilized in this study. It is assumed that the flow of fluid from each pore throat at the i-th flow path level to each pore throat at the $(i+1)$-th flow path level takes place not only from the two contiguous pore necks and bodies which are connected to each pore throat at the i-th flow path level, but also from the other noncontiguous pore necks and bodies which are not connected to each pore throat at the i-th flow path level (see Fig. 1). Note that, the porous model in Fig. 1 has been chosen arbitrarily to demonstrate this assumed flow path mode (the model in Fig. 1 is not the porous medium used in the experiments of this study. The reason to use this specific model in Fig. 1 – and not the actual micromodel pattern that was used in the experiments – is because of its pattern simplicity in terms of orientation of the pore bodies and necks in a way that it allows us to demonstrate the PNA concept in a more clear way). Therefore, $f(i)$ can be written as [50]:

$$f(i) = \frac{i[4+2(i-1)]}{2} = i(i+1), 1 \leqslant i \leqslant n \tag{3}$$

From Eqs. (1)–(3), it can be concluded that the calculation of the pore-scale capillary number will be dependent on the assumed flow path mode. Hence, according to the defined relationship for the average interstitial velocity of the displacing non-wetting phase Eqs. (2) and (3), dynamic mean pore-scale capillary numbers can be calculated for each flow path level (i.e., for each "n"). Hence, by combining Eqs. (1)–(3), the following relation can be written to estimate the dynamic mean pore-scale capillary number [50]:

$$N_{c_1} = \frac{\mu_d Q_{inj}\sum_{i=1}^{n}\frac{1}{i(i+1)}}{hd_t n\sigma\cos\theta}. \tag{4}$$

Table 5
Physical and hydraulic properties of the micromodel.

Length and width (mm)	Pore diameter (μm)	Throat diameter (μm)	Coordination number	Aspect ratio	Absolute permeability (m^2)	Porosity (fraction)	Average etched thickness (μm)
60	647 ± 25	280 ± 15	3	2.31	$(2.05 \pm 0.11)\times10^{-12}$	0.4082	31

Eq. (4) predicts the dynamic mean pore-scale capillary number by excluding the potential effects of the viscous instability on the physics of the flow, i.e., mainly wetting phase (i.e., oil) bypassing and trapping. The next subsection provides a way of predicting the dynamic mean pore-scale capillary number by including the potential effects of the viscous instability, which are wetting phase bypassing and trapping.

3.2. Determination of the pore-scale capillary number using viscous instability model

A quantity that is often used in the instability analysis is the wavelength of the fingers. Theoretically, in immiscible two-phase flow displacements in a cylindrical core, the finger wavelength is short at a high displacement rate, which results in the accommodation of numerous fingers by the core. By comparison, the finger wavelength is longer at lower rates, and thus, a few fingers can be accommodated. Thus, the wavelength of the fingers is a strong function of the rock and fluid properties and displacement rate. Peters and Flock [49] obtained a dimensionless scaling group and its critical value for predicting the onset of instability during two-phase immiscible displacement in porous media. They related the wavelength of the developed viscous fingers (λ_m) to the physical properties of the two fluids and the porous medium by the following relationship [49]:

$$\lambda_m = C\left(\frac{k\sigma}{(\mu_o - \mu_d)\,u}\right)^{0.5}. \tag{5}$$

where C is the wettability number ($\approx$25 for an oil-wet porous medium), k is the absolute permeability (m^2), and μ_o is the dynamic viscosity of the displaced wetting phase. The wettability number is a dimensionless number that can be used to relate the effective interfacial tension to the liquid/liquid interfacial tension in prediction of the onset of instability. This number also quantifies the ability of the porous medium to imbibe the displacing phase. In an oil-wet medium, for example, the wettability number is smaller than that in a water-wet medium because the imbibition forces are relatively smaller in an oil-wet medium. The wettability number can be determined experimentally for different wettability states once the fastest growing finger wavelength is measured in an experiment [49].

Combining Eqs. (1) and (5), and rearranging for the N_{c1} give:

$$N_{c1} = \frac{C^2 k \mu_d}{\lambda_m^2 (\mu_o - \mu_d)\varphi \cos\theta}. \tag{6}$$

Eq. (6) predicts the dynamic mean pore-scale capillary number based on the viscous instability model (VIM). In VIM, the effect of viscous instability, which causes the wetting phase (i.e., oil) bypassing and trapping, is considered in determining the values of the dynamic mean pore-scale capillary number. The latter is possible by determining the values of the wavelength of the developed viscous fingers (λ_m) at any time of the displacement utilizing flow visualization techniques (see Section 4). Therefore, unlike the simplified pore network approach (PNA) that was discussed in Section 3.1, the effect of viscous instability is quantified using Eq. (6) in order to predict the dynamic mean pore-scale capillary number. In other words, Eq. (4) predicts the dynamic mean pore-scale capillary number by excluding the effects of viscous instability. Hence, comparison between the dynamic mean pore-scale capillary numbers obtained from Eqs. (4) and (6) can be used to quantify the effect of viscous instability on the physics of flow. This comparison provides an insight into the effects of viscous instability on the relative change of the viscous-to-capillary forces in viscous-modified low-IFT flow with adverse mobility ratio through an initially preferential oil-wet porous medium. Furthermore, using this approach, the effects of salinity of the displacing non-wetting phase on the physics of flow can be investigated.

4. Results and discussion

4.1. Effect of salinity on the IFT, viscosity, and contact angle

The values of the displacing phase–displaced phase IFT, displacing phase viscosity, and contact angle at different salinities of the displacing non-wetting phase are given in Table 4. The decreasing trend of the displacing phase viscosity by increase in the salinity of the displacing phase is self-evident in Table 4. In addition, the displacing phase–displaced phase IFT increases by increase in the salinity of the displacing non-wetting phase. The measured values of the contact angle reported in Table 4 show an increasing trend by increase in the salinity of the displacing non-wetting phase. It is worth noting that the contact angles were measured using the sessile drop method.

4.2. Effect of salinity on the displacement front configuration

The dynamic advance of the displacement front configuration at different salinities of the displacing non-wetting phase is given in Fig. 2–4. The salinity of the displacing non-wetting phase increases from Run #1 to Run #3. These three figures show that the qualitative features of the displaced wetting phase bypassing and trapping at different salinity levels of the displacing non-wetting phase are significantly different. Therefore, the salinity of the displacing non-wetting phase dramatically influences the wetting phase trapping and bypassing in viscous-modified low-IFT flow with adverse mobility ratio through initially preferential oil-wet porous media. The second general finding from the images of the displacement front configuration is the cause of the viscous insta-

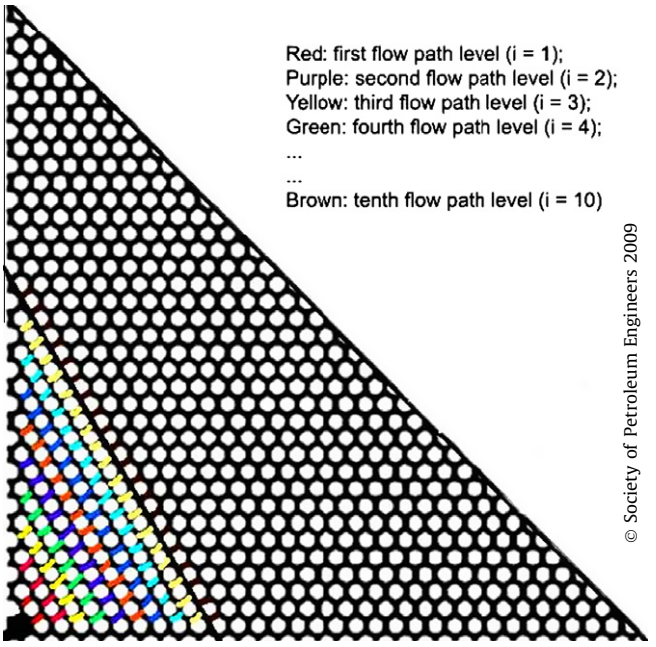

Fig. 1. Idealized flow path mode in the simplified pore network approach, (reproduced from Ref. [50] with permission of the copyright owner. Further reproduction prohibited without permission). For example, red color corresponds to the first flow path level or when $i = 1$, yellow color corresponds to the third flow path level or when $i = 3$, and so on. (For interpretation of the references to colour in this figure legend, the reader is referred to the web version of this article.)

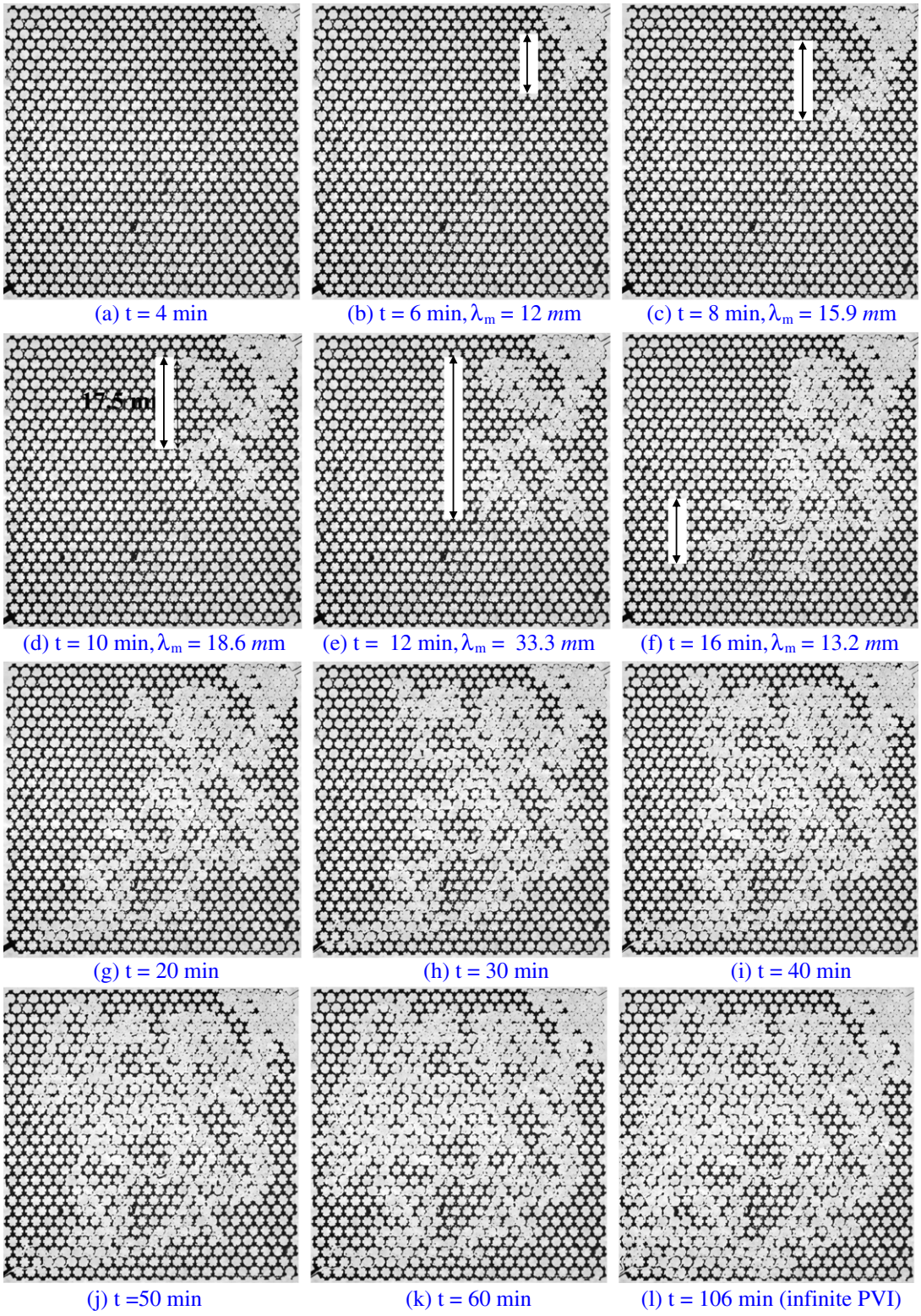

Fig. 2. Displacement front configuration in Run #1.

bility in viscous-modified low-IFT flow. To be more precise, regardless of the salinity level of the displacing non-wetting phase, dynamic cluster-growth nature of the advancing displacement front is the main cause of the occurrence of viscous instability in the conducted runs. However, at higher salinity levels of the displacing non-wetting phase, the effect of dynamic cluster-growth nature of the advancing displacement front is more pronounced before channeling and consequent breakthrough of the tongue of the displacing non-wetting phase to the production site.

It is readily observed that the salinity of the displacing non-wetting phase has a direct effect on the onset of instability in viscous-modified low-IFT flow with adverse mobility ratio. Figs. 2–4 show that decrease in the salinity of the displacing non-wetting phase delays the onset of viscous instability in an initially

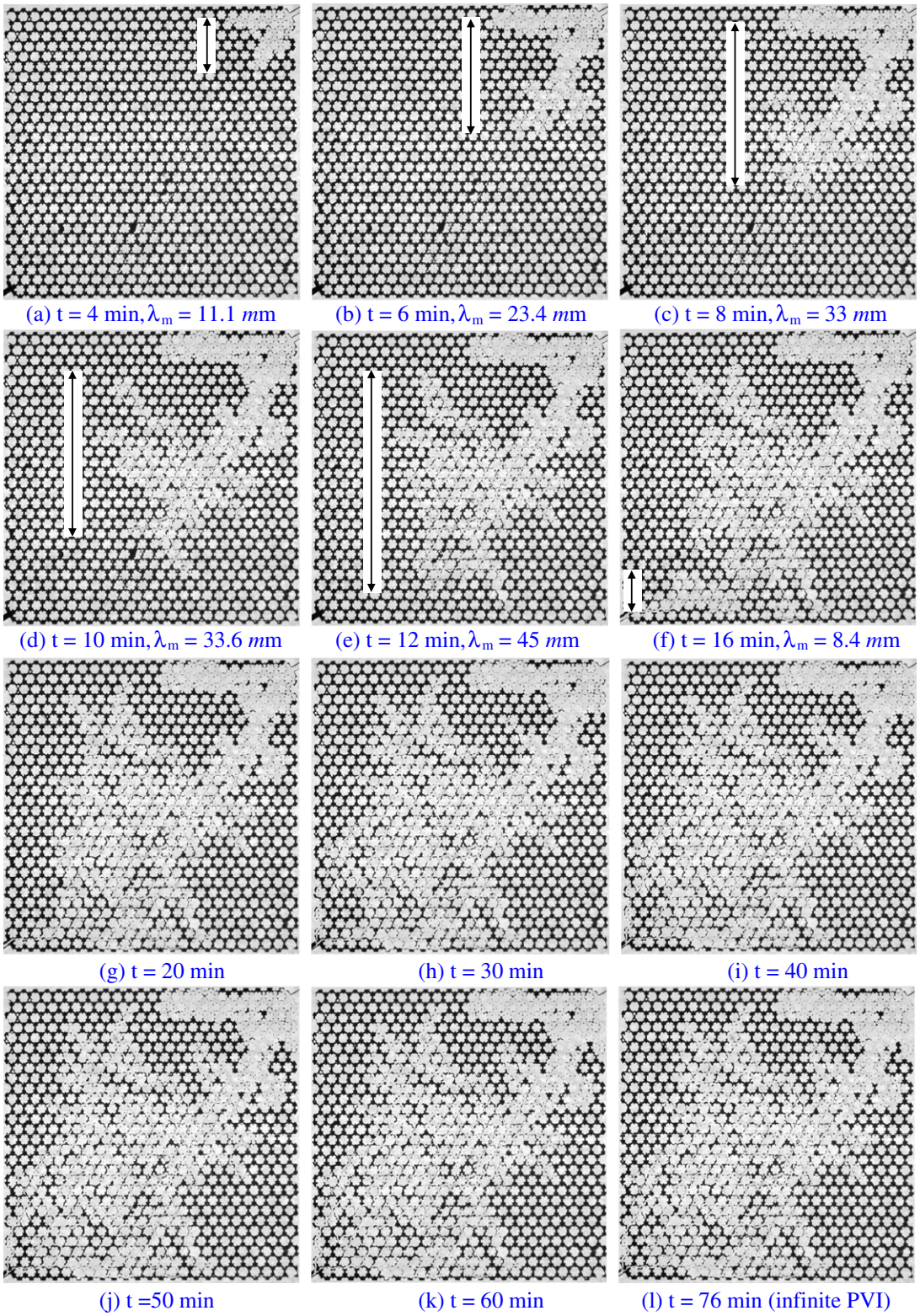

Fig. 3. Displacement front configuration in Run #2.

preferential oil-wet porous medium (see Figs. 2a, 3a, and 4a). In addition, at the early stages of the displacement, by increase in the salinity of the displacing non-wetting phase, the viscous instability becomes more severe before breakthrough of the displacing phase (see and compare Fig. 2b, 2c, 3b, 3c, 4b, 4c). Another important observation from the configuration of the displacement front is that by increase in the salinity of the displacing non-wetting phase in viscous-modified low-IFT flow, the tongue of the displacing fluid channels earlier to the production site (compare Figs. 2g, 3f, and 4d). One of the most important observations regarding the displacement front configuration is witnessing a relatively less noticeable change in the viscous instability patterns after breakthrough by increase in the salinity of the displacing non-wetting phase (see Figs. 2–4). To be more precise, by increase in the salinity

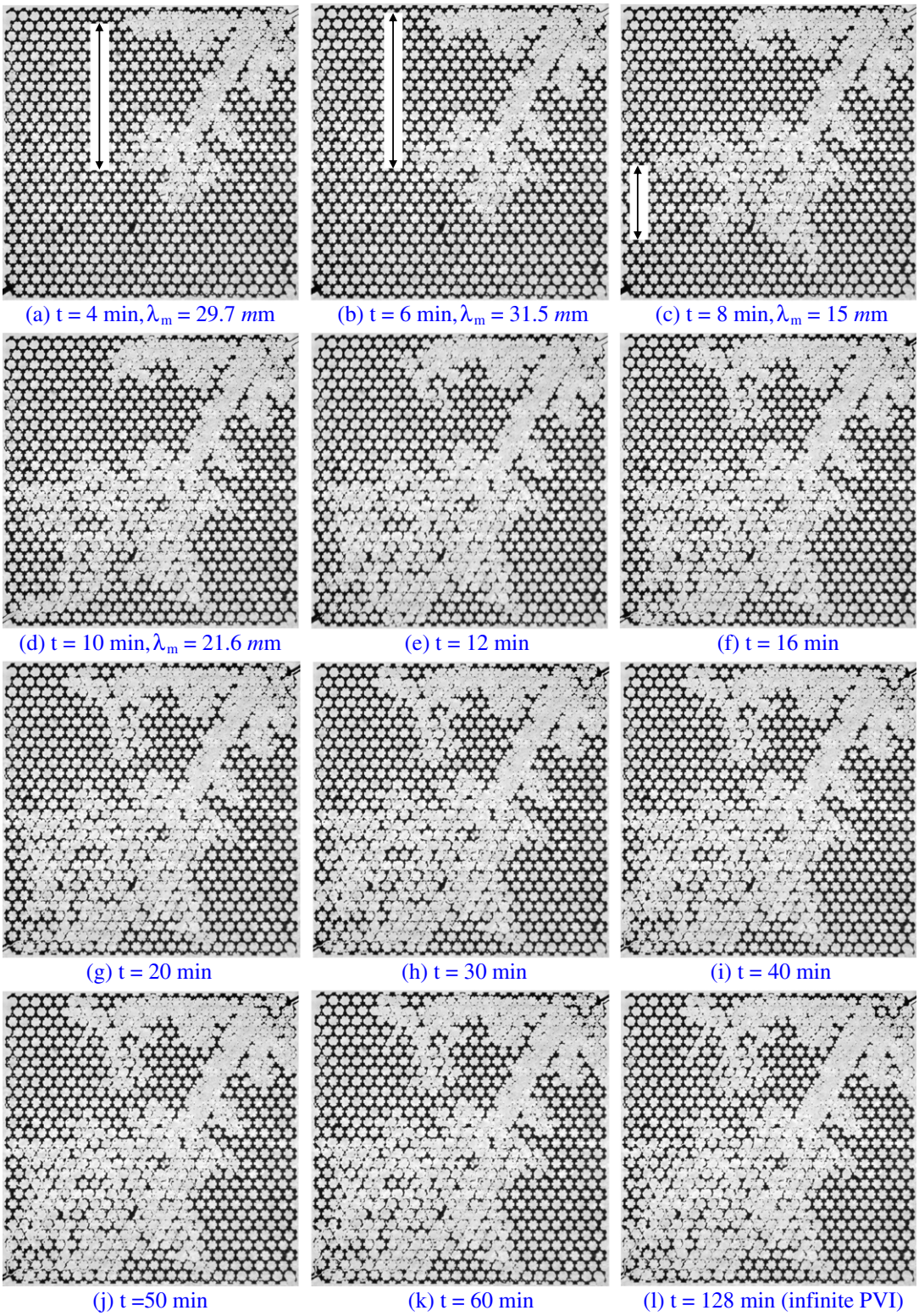

Fig. 4. Displacement front configuration in Run #3.

of the displacing non-wetting phase, change in viscous fingering patterns from breakthrough to the time of infinite injected pore volume (IPV) becomes relatively less noticeable. When the salt concentration is zero within the displacing phase, the flow patterns change dramatically after breakthrough (see Fig. 2h-l). This tendency exists on a relatively lower level by increase in the salinity of the displacing phase (Fig. 3f-l) and is minimized by further increase in the salinity of the displacing phase (Fig. 4e-l).

4.3. Effect of salinity on the wavelength of the developed viscous fingers

In order to investigate the effects of the salinity of the displacing non-wetting phase on the wavelength of the developed viscous fingers, images of the displacement front before breakthrough were captured under a high-resolution digital camera. These images are given in Figs. 2b–f, 3a–f, and 4a–c for an initially preferential

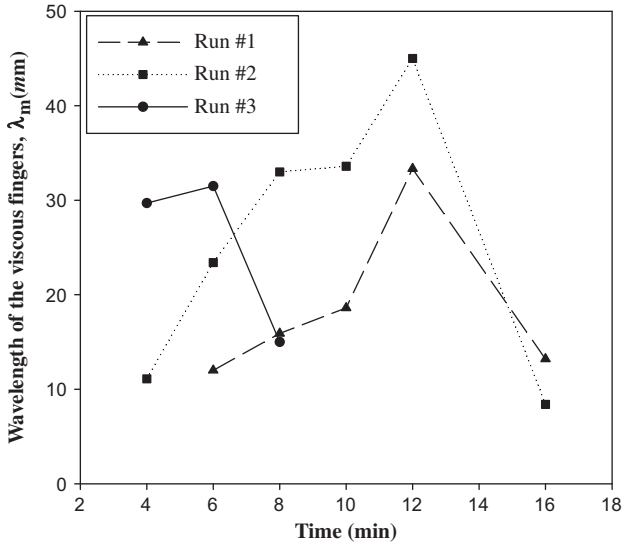

Fig. 5. Effect of salinity on λ_m.

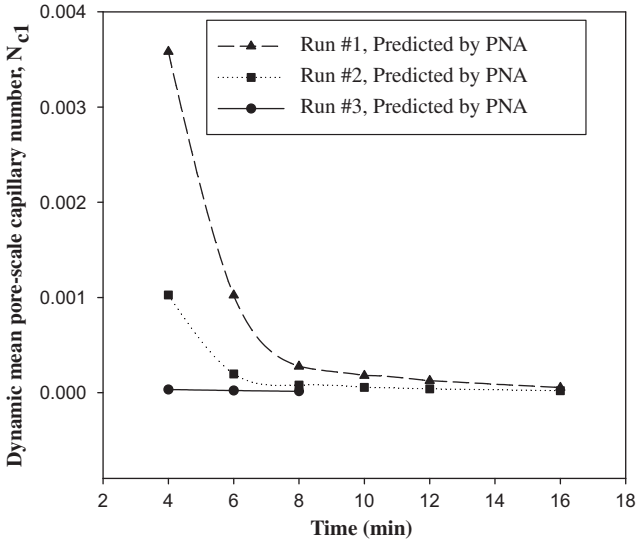

Fig. 6. Effect of salinity on N_{c1} in PNA.

oil-wet porous medium. The values of the wavelength of the developed viscous fingers, λ_m, have been measured using image analysis. These values are indicated by arrows in these figures. Figs. 2b–f, 3a–f, and 4a–c suggest one important conclusion in viscous-modified low-IFT flow through oil-wet porous media: regardless of the salinity level, the wavelength of the developed viscous fingers increases dynamically until near breakthrough of the displacing non-wetting phase; afterwards, wavelength of the developed viscous fingers decreases suddenly and the developed tongue of the displacing non-wetting phase channels to the production site.

The dynamic changes in the values of the wavelength of developed viscous fingers, by advance of the displacement front, at different salinities of the displacing non-wetting phase are given in Fig. 5. Comparing Figs. 2a and b, 3a and b, 4a and b, one can conclude that at the early stages of the displacement, wavelength of the developed viscous fingers increases by increase in the salinity of displacing non-wetting phase. This is in good qualitative agreement with the proposed relation of the Peters and Flock [49], which predicts the wavelength of the developed viscous fingers. In the original model of the onset of instability in two-phase immiscible displacement in porous media, it was proposed that the wavelength of the developed viscous finger is inversely proportional to the square root of the average superficial velocity of the displacing fluid [49]. It is also observed that in absence of salts in the displacing phase, the dynamic growth of the wavelength of developed viscous fingers of the displacing non-wetting phase is relatively uniform (see Figs. 5 and 2b–e). On the contrary, in the presence of salts, the trend of the dynamic growth of the developed viscous fingers is relatively nonuniform.

4.4. Effects of salinity on the dynamic mean pore-scale capillary number resulting from pore network approach: Excluding the viscous instability effect

Eq. (4) was used to determine the dynamic mean-pore scale capillary number values by neglecting the viscous instability effects. These values are reported in Table 6. Fig. 6 and Table 6 illustrate the effects of salinity of the displacing non-wetting phase on the dynamic mean pore-scale capillary number in viscous-modified low-IFT flow with adverse mobility ratio, through an initially preferential oil-wet porous medium. These dynamic mean pore-scale capillary number values were obtained from the pore network approach, which excludes the viscous instability effects. Table 6 shows the dynamic mean pore-scale capillary numbers predicted by the PNA where the viscous instability effects are neglected. These dynamic mean pore-scale capillary numbers lie in the range of 10^{-5}–10^{-3}. The first general finding from these data in Fig. 6 and Table 6 is the decrease in the dynamic mean pore-scale capillary number by the increase in the salinity of the displacing phase. Another general concluding remark from this figure is that regardless of the salinity level of the displacing phase, dynamic mean pore-scale capillary number values decrease nonuniformly by advance of the displacement front.

From Fig. 6 and Table 6, it can readily be inferred that during the early stages of the displacement (4–6 min), the difference between the dynamic mean pore-scale capillary numbers at different salinities is very significant. Fig. 6 shows that this difference becomes less noticeable as the displacement front proceeds. Finally, it is minimized near the breakthrough of the displacing phase. Furthermore, at lower salinities, the relative decrease in the dynamic mean

Table 6
Predicted dynamic mean pore-scale capillary number by the pore network approach at different times before breakthrough of the displacing non-wetting phase (Q_{inj} = 0.0008 cm^3/min).

Run No.	Dynamic mean pore-scale capillary number N_{c1}					
	t = 4 min	t = 6 min	t = 8 min	t = 10 min	t = 12 min	t = 16 min
1	$n \approx 3$	$n \approx 6$	$n \approx 12$	$n \approx 15$	$n \approx 18$	$n \approx 28$
	0.0035824	0.0010235	0.0002756	0.0001791	0.0001257	5.29E−05
2	$n \approx 5$	$n \approx 12$	$n \approx 19$	$n \approx 23$	$n \approx 27$	$n \approx 38$
	0.0010265	0.0001974	8.10E−05	5.58E−05	4.07E−05	2.08E−05
3	$n \approx 19$	$n \approx 23$	$n \approx 29$	–	–	–
	3.33E−05	2.30E−05	1.46E−05	–	–	–

Table 7
Predicted dynamic mean pore-scale capillary number by the viscous instability model at different times before breakthrough of the displacing non-wetting phase (Q_{inj} = 0.0008 cm^3/min).

Run No.	Dynamic mean pore-scale capillary number N_{c1}					
	t = 4 min	t = 6 min	t = 8 min	t = 10 min	t = 12 min	t = 16 min
1	–	2.68E−06	1.53E−06	1.12E−06	3.5E−07	2.21E−06[a]
2	2.48E−06	5.6E−07	2.8E−07	2.7E−07	1.5E−07	4.34E−06[a]
3	1.7E−07	1.5E−07	6.6E−07[a]	–	–	–

[a] Dynamic mean pore-scale capillary number just before the breakthrough.

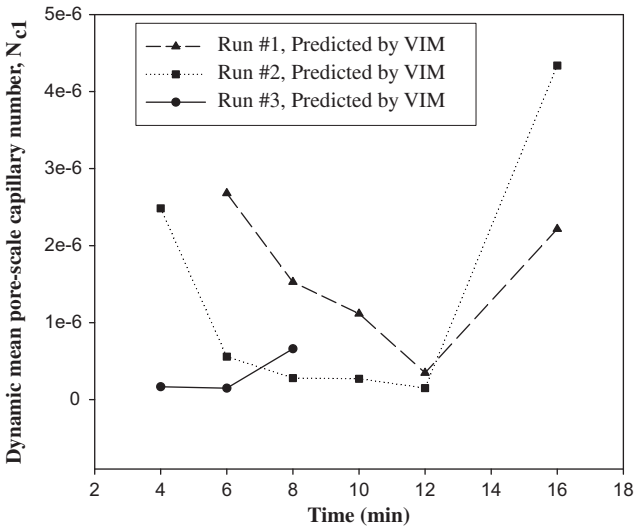

Fig. 7. Effect of salinity on N_{c1} in VIM.

pore-scale capillary numbers by advance of the displacement front is more pronounced. According to the predictions in the absence of the viscous instability effects, by increase in the salinity, the decrease in the dynamic mean pore-scale capillary number (by advance of the displacement front) becomes relatively less noticeable.

4.5. Effect of salinity on the dynamic mean pore-scale capillary number resulting from viscous instability model: Including the viscous instability effect

The resulting values of the dynamic mean pore-scale capillary number in viscous-modified low-IFT flow with adverse mobility ratio, through an initially preferential oil-wet porous medium, from viscous instability model are given in Table 7 and Fig. 7. These values are reported at different salinity levels of the displacing non-wetting phase. Eq. (6) was used to determine the reported dynamic mean pore-scale capillary number values by considering the viscous instability effects. The dynamic mean pore-scale capillary numbers determined by considering the viscous instability effects are in the range of 10^{-7}–10^{-6}. By comparing the corresponding dynamic mean pore-scale capillary number values reported in Tables 6 and 7, it is concluded that neglecting the viscous instability effects in Eq. (4) causes the overestimation of the dynamic mean pore-scale capillary number values in PNA. This overestimation is evident by one to three orders of magnitude. The severe overestimation of the dynamic mean pore-scale capillary numbers with three orders of magnitude is observed during the early stages of the displacement (t = 4 and t = 6 min) for the lower salinities. Tables 7 and 8 show that by increase in the salinity of the displacing phase, the level of overestimation of the dynamic mean pore-scale capillary number values during the early stages of the displacement (t = 4 and t = 6 min) in absence of viscous instability effects relatively decreases. The order of magnitude of this overestimation is reduced to two at the relatively highest salinity level of the displacing phase. In general, at the lower salinities (Runs #1 and #2), the difference between the dynamic mean pore-scale capillary number values obtained from the PNA and VIM decreases as the displacement proceeds. This difference is minimized and it reaches to one order of magnitude just before the breakthrough. This means that at lower salinity levels of the displacing phase, by advance of the displacement front, the effects of viscous instability on dynamic mean-pore scale capillary number becomes relatively less noticeable. On the contrary, at the relatively highest salinity level (Run #3), the viscous instability effect remains constant. At the highest salinity of the displacing phase, the difference between the dynamic mean pore-scale capillary numbers resulted from the PNA and VIM remains constant (two orders of magnitude).

Table 8
Breakthrough time and infinite IPV time of the displacing non-wetting phase.

Run No.	Breakthrough time (min)	Infinite IPV time (min)
1	21	106
2	16.20	76
3	8.80	128

Fig. 7 illustrates the effects of salinity on the dynamic mean pore-scale capillary number in viscous-modified low-IFT flow with adverse mobility ratio including the viscous instability effects. These values are those reported in Table 7. The first general finding from Fig. 7 is the decrease in the dynamic mean pore-scale capillary number by increase in the salinity of the displacing phase except near the breakthrough. This is against the predictions by the PNA in Fig. 6. Therefore, including the viscous instability effects disturbs the predicted trends of the dynamic mean pore-scale capillary number values near breakthrough. In PNA, regardless of the salinity level of the displacing phase, dynamic mean pore-scale capillary number values decrease nonuniformly by advance of the displacement front (see Fig. 6). On the contrary, in VIM, this trend is disturbed; and values of the dynamic mean pore-scale capillary number initially decrease by advance of the displacement front; afterward, they increase near breakthrough. In PNA, at the early stages of the displacement (t = 4–6 min), the difference between the dynamic mean pore-scale capillary numbers at different salinities becomes less noticeable as the displacement front proceeds and it is minimized near the breakthrough. In VIM, this difference is generally pronounced during the entire displacement. As opposed to the PNA, the difference between the dynamic mean pore-scale capillary numbers predicted by the VIM at different salinities is maximized near the breakthrough.

The analysis of the viscous instability effects reveals that the behavior of the viscous-modified low-IFT flow through an oil-wet porous medium becomes very complex, especially near breakthrough of the displacing non-wetting phase. Therefore, including the viscous instability effects in qualitative and quantitative evaluations of the viscous-modified low-IFT flow occurring in the surfactant–polymer flooding of heavy oil reservoirs is vital.

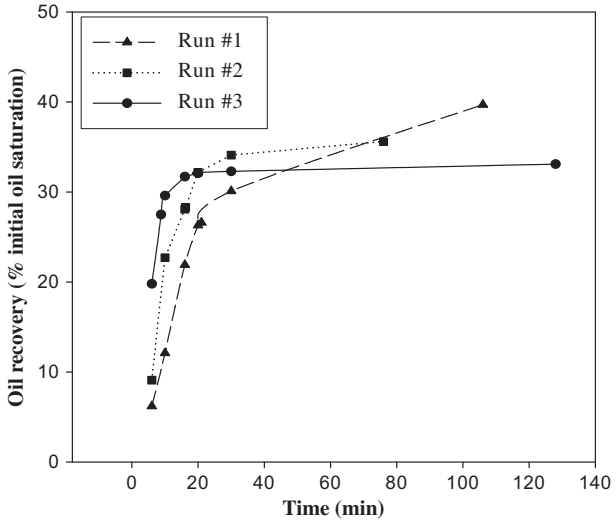

Fig. 8. Effect of salinity on oil recovery.

4.6. Effect of salinity on the oil recovery, breakthrough time, and time of infinite IPV

Fig. 8 shows the effect of salinity of the displacing non-wetting phase on values of the desaturated displaced wetting phase (i.e., heavy oil recovery). This figure shows that by increase in the salinity of the displacing non-wetting phase, values of the desaturated displaced wetting phase at infinite IPV (i.e., ultimate oil recovery) decrease. During the early stages of the displacement and before the breakthrough, increase in the salinity causes an increase in the values of the desaturated displaced wetting phase. Afterwards, after the breakthrough this trend is disturbed. Finally, at infinite IPV of the displacing phase, the trend of desaturated displaced wetting phase is contrary to that during the early stages of the displacement process.

Table 8 shows the breakthrough time and infinite IPV time of the displacing non-wetting phase. As it is reported, the breakthrough time of the displacing wetting phase decreases by increase in the salinity. Therefore, the displacing non-wetting phase channels earlier to the production site by increase in the salinity. Also, Table 8 shows that by increase in the salinity, infinite IPV time decreases initially. However, at the highest salinity level, the infinite IPV time increases and it exceeds that of Run #1 where no salts are present within the displacing phase.

5. Summary and conclusions

1. The dynamic cluster-growth nature of the front is the main cause of viscous instability. The wavelength of the viscous fingers increases dynamically until near the breakthrough; afterwards, wavelength of the developed viscous fingers suddenly decreases. In the presence of salts, the dynamic growth of the viscous fingers is nonuniform. Also, a less noticeable change in the instability patterns was observed after breakthrough by increase in the salinity. Furthermore, during the early stages of the displacement, wavelength of the developed viscous fingers increases by increase in the salinity. Decrease in salinity delays the onset of instability.
2. In PNA, the dynamic mean pore-scale capillary numbers predicted by excluding the viscous instability effects are in the range of 10^{-5}–10^{-3} and they decrease nonuniformly by the advance of the displacement front and the increase in the salinity. At the early stages, the difference between the dynamic mean pore-scale capillary numbers at different salinities is significant; it then becomes smaller as the displacement proceeds and is minimized near the breakthrough.
3. In VIM, the dynamic mean pore-scale capillary numbers predicted by including the viscous instability effects are in the range of 10^{-7}–10^{-6}. Thus, neglecting the viscous instability effects overestimates the dynamic mean pore-scale capillary numbers in PNA. The overestimation is severe during the early stages for the lower salinities.
4. Including the viscous instability effects disturbs the predicted trends of the dynamic mean pore-scale capillary numbers in PNA near the breakthrough. In PNA, the difference between the dynamic mean pore-scale capillary numbers becomes less noticeable as the displacement proceeds and is minimized near the breakthrough. In VIM, however, this difference is pronounced during the entire displacement and is maximized near the breakthrough.
5. During the early stages, increase in the salinity increases oil recovery. This trend is disturbed near the breakthrough, and at infinite IPV, oil recovery decreases by increase in the salinity.

Acknowledgements

BYJ and KA acknowledge the support provided by the Petroleum Technology Research Centre, Regina. Also, BYJ thanks the Petroleum Research Center at the Petroleum University of Technology, Tehran, for providing the laboratory facilities and the Research and Development Directorate of the National Iranian Oil Company for the financial support in conducting the experiments.

References

[1] Yadali Jamaloei B. Experimental study of surfactant/water/polymer flooding using one-quarter five-spot glass micromodels. M.Sc. thesis. Tehran, Iran: Petroleum University of Technology; 2007.
[2] Yadali Jamaloei B. Recent Patents. Chem Eng 2009;2:1–10.
[3] Yadali Jamaloei B, Ahmadloo F, Kharrat R. Fluid Dyn. Res. 2010;42:055505.
[4] Yadali Jamaloei B, Kharrat R. Trans Porous Media 2010;81:1–19.
[5] Yadali Jamaloei B, Kharrat R. J Porous Media 2011;14(2):91–105.
[6] Yadali Jamaloei B, Asghari K, Kharrat R. Exp Therm Fluid Sci 2011;35:253–64.
[7] Bansal VK, Shah DO. J Am Oil Chem Soc 1978;55:367–70.
[8] Bansal VK, Shah DO. J Colloid Interface Sci 1978;65:451–9.
[9] Glover CJ, Puerto MC, Maerker JM, Sandvik EL. Soc Petrol Eng J 1979;19:183–93.
[10] Gupta SP, Trushenski SP. Soc Petrol Eng J 1979;19:116–28.
[11] Hirasaki GJ. Soc Petrol Eng J 1981;21:191–204.
[12] Celik MS, Manev ED, Somasundaran P. Interfacial phenomena in enhanced oil recovery. AIChE Symp 1982;212:86–96.
[13] Hirasaki GJ. Soc Petrol Eng J 1982;22:971–82.
[14] Kraft HR, Pusch G. SPE enhanced oil recovery symposium, 1982; Tulsa, Oklahoma, USA.
[15] Nelson RC. Soc Petrol Eng J 1982;22:259–70.
[16] Hirasaki GJ, van Domselaar HR, Nelson RC. Soc Petrol Eng J 1983;23:486–500.
[17] Sharma AK, Shah DO. SPE oilfield and geothermal chemistry symposium, 1983, Denver, Colorado, USA.
[18] Kumar A, Neale GH, Hornof V. J Can Petrol Technol 1984;23:37–41.
[19] Kumar A, Neale G, Hornof V. J Colloid Interface Sci 1985;104:130–5.
[20] Hirasaki GJ, Lawson JB. Soc Petrol Eng Reservoir Eng 1986;1:119–30.
[21] Pithapurwala YK, Sharma AK, Shah DO. J Am Oil Chem Soc 1986;63:804–13.
[22] Leung R, Shah DO. J Colloid Interface Sci 1987;120:330–44.
[23] Chou SI, Bae JH. Soc Petrol Eng Reservoir Eng 1988;3:778–90.
[24] Agharazi-Dormani N, Hornof V, Neale GH. J Petrol Sci Eng 1990;4:189–96.
[25] Anton RE, Salager JL. J Colloid Interface Sci 1990;140:75–81.
[26] Badakshan A. SPE Paper No. 20295-MS; 1990.
[27] Porzucek C, Ramirez WF. J Petrol Sci Eng 1990;4:335–45.
[28] Miller DJ, von Halasz S-P, Schmidt M, Holst A, Pusch G. J Petrol Sci Eng 1991;6:63–72.
[29] Noll LA. SPE international symposium on oilfield chemistry, 1991. Anaheim, California, USA.
[30] Barker JW. J Petrol Sci Eng 1992;7:139–54.
[31] Maerker JM, Gale WW. Soc Petrol Eng Reservoir Eng 1992;7:36–44.
[32] Abuin EB, Rubio MA, Lissi EA. J Colloid Interface Sci 1993;158:129–32.
[33] Carlsson I, Edlund H, Persson G, Lindström B. J Colloid Interface Sci 1996;180:598–604.
[34] Fjelde I, Austad T, Milter J. J Petrol Sci Eng 1995;13:193–201.

[35] Kaczmarski JP, Tarng M-R, Ma Z, Glass JE. Colloid Surface Physicochem Eng Aspect 1999;147:39–53.
[36] Hou Z, Li Z, Wang H. J Dispers Sci Technol 2001;22:255–9.
[37] Ström C, Jönsson B, Söderman O. J Dispers Sci Technol 2001;22:387–96.
[38] Wang Y, Wang L, Li J, Zhao F. SPE Permian basin oil and gas recovery conference, 2001, Midland, Texas, USA.
[39] Al-Sahhaf T, Elkamel A, Suttar Ahmed A, Khan AR. Chem Eng Commun 2005;192:667–84.
[40] Li G-Z, Xu J, Mu J-H, Zhai L-M, Shui L-L, Chen W-J, et al. J Dispers Sci Technol 2005;26:709–17.
[41] Mitra T, Ghosh P. J Dispers Sci Technol 2007;28:785–92.
[42] Para G, Warszynski P. Colloid Surface Physicochem Eng Aspect 2007;300:346–52.
[43] Yadali Jamaloei B, Asghari K, Kharrat R, Ahmadloo F. J Petrol Sci Eng 2010;72:251–69.
[44] Yadali Jamaloei B, Kharrat R. Transp Porous Media 2009;76:199–218.
[45] Yadali Jamaloei B, Kharrat R. J Porous Media 2010;13:671–90.
[46] Yadali Jamaloei B, Kharrat R, Torabi F. Energy Fuels 2010;24:6384–92.
[47] Yadali Jamaloei B, Kharrat R, Torabi F. Canadian unconventional resources and international petroleum conference Calgary. Canada: AB; 2010.
[48] Yadali Jamaloei B, Rafiee M. Canadian international petroleum conference Calgary. Canada: AB; 2008.
[49] Peters EJ, Flock DL. Soc Petrol Eng J 1981;21:249–58.
[50] Yadali Jamaloei B, Kharrat R, Ahmadloo F. SPE Kuwait international petroleum conference and exhibition 2009, Kuwait City, Kuwait.